Self and Transport Diffusivity of CO_2 in the Metal−Organic Framework MIL-47(V) Explored by Quasi-elastic Neutron Scattering Experiments and Molecular Dynamics Simulations

Fabrice Salles,[†] Hervé Jobic,[‡,*] Thomas Devic,[§] Philip L. Llewellyn,[⊥] Christian Serre,[§] Gérard Férey,[§] and Guillaume Maurin[†,*]

[†]Institut Charles Gerhardt Montpellier, UMR CNRS 5253, UM2, ENSCM, Université Montpellier 2, Place E. Bataillon, 34095 Montpellier Cedex 05, France, [‡]Institut de Recherches sur la Catalyse et l'Environnement de Lyon, Université de Lyon CNRS, 2 Avenue A. Einstein, F-69626 Villeurbanne, France, [§]Institut Lavoisier, UMR CNRS 8180, Université Versailles-Saint-Quentin-en-Yvelines, 78035 Versailles, France, and [⊥]Laboratoire Chimie Provence, Université Aix-Marseille I, II, and III-CNRS-UMR 6264, Centre de Saint-Jérôme, 13397 Marseille, France

ABSTRACT Quasi-elastic neutron scattering measurements are combined with molecular dynamics simulations to determine the self-diffusivity, corrected diffusivity, and transport diffusivity of CO_2 in the metal−organic framework MIL-47(V) (MIL = Materials Institut Lavoisier) over a wide range of loading. The force field used for describing the host/guest interactions is first validated on the thermodynamics of the MIL-47(V)/CO_2 system, prior to being transferred to the investigations of the dynamics. A decreasing profile is then deduced for D_s and D_0 whereas D_t presents a non monotonous evolution with a slight decrease at low loading followed by a sharp increase at higher loading. Such decrease of D_t which has never been evidenced in any microporous systems comes from the atypical evolution of the thermodynamic correction factor that reaches values below 1 at low loading. This implies that, due to intermolecular interactions, the CO_2 molecules in MIL-47(V) do not behave like an ideal gas. Further, molecular simulations enabled us to elucidate unambiguously a 3D diffusion mechanism within the pores of MIL-47(V).

KEYWORDS: metal−organic framework · self-diffusivity · corrected diffusivity · transport diffusivity · QENS · molecular dynamics · CO_2

The economically viable capture of carbon dioxide appears clearly as a priority to reduce global warming caused by the emission of greenhouse gases and to favor the emergence of the future world economy based on hydrogen as an energy vector.[1,2] Advances in reducing CO_2 emissions may thus lead to a number of potential benefits in different fields related to both energy development and environmental protection. Such environmental and economical problems that society faces today have galvanized the research for novel competitive nanoporous materials able to efficiently adsorb CO_2.[1,3] To that purpose, the metal−organic framework (MOF) materials appear as promising alternative candidates to zeolites and activated carbons, currently used as adsorbents in PSA-based systems.[4−6] Indeed, MOFs exhibit very attractive features for the adsorption of various gases including H_2,[7−12] CH_4, and CO_2.[7,13−16] For instance, a very high CO_2 adsorption uptake has been highlighted for the MIL-101 solid.[17] Further, some MOFs are able to breathe in the presence of specific probe molecules which can open up an interesting way to efficiently control selective gas adsorption.[3,18−21] Experimental and theoretical studies have generally focused on the adsorption/diffusion of H_2 in different MOFs.[11,22−25] In contrast, fewer experimental explorations have been dedicated to CO_2 adsorption properties of these materials.[5,17,26−31] Nevertheless, several studies have been devoted to the MIL-series (MIL-53(Cr), MIL-47(V), MIL-100 (Cr), and MIL-101 (Cr)),[17,27] MOF-508b[30] as well as to other MOFs systems recently synthesized such as $Zn_2(NDC)_2(DPNI)$ (where NDC = 2,6-naphthalenedicarboxylate, DPNI = *N*,*N*′-di-(4-pyridil-1,4,5,8-naphthalen tetracarboxydiimide)[26] and CPO-27 or $Ni_2(dhtp)$ (where H_4dhtp = 2,5-dihydroxyterephthalic acid; CPO = coordination polymer from Oslo)[29] solids. They were completed by molecular simulations at different levels of theory including thermodynamics models.[32] Using the quantum chemical approach, the geometric and energetic nature of the CO_2/MOF framework interactions were deduced.[32,33] Classical simulations based

*Address correspondence to gmaurin@lpmc.univ-montp2.fr, herve.jobic@ircelyon.univ-lyon1.fr.

Received for review September 1, 2009 and accepted November 27, 2009.

Published online December 3, 2009. 10.1021/nn901132k

© 2010 American Chemical Society

on Monte Carlo simulations and reliable force field were also conducted to probe the CO_2 adsorption in various rigid MOFs[34−36] and more scarcely in flexible solids which exhibit significant structural modifications upon adsorption as typically observed in the MIL-53 system.[34,37,38] Molecular dynamics have also been employed to follow the dynamics of CO_2 in various MOFs. Skoulidas *et al.*[39] and Babarao *et al.*[40] thus predicted the evolutions of both transport diffusivity(D_t) and self (D_s)-diffusivity as a function of CO_2 loading in MOF-5. More recently, Yang *et al.*[41] focused their investigations on the self-diffusivity in various MOFs including IRMOF-10, IRMOF-14, and MOF-177. The dynamics of CO_2 of one order of magnitude greater than in usual zeolites was reported, which reinforces the potential interest of these materials for applications in the field of gas storage. However, none of these simulations were compared to experimental data.

The main interest of our work here is to combine adapted theoretical and experimental tools able to probe both individual and collective CO_2 dynamics in a typical MOF system *via* the determination of the self-diffusivity (D_s) and transport (D_t) diffusivity, respectively. While the self-diffusivity describes the displacements of individual tagged molecules, the transport diffusivity, commonly referred to as the Fickian diffusivity or collective diffusivity, is related to a mass transport induced by a macroscopic gradient in the chemical potentials of the considered species.[42,43] Indeed, when one investigates industrial applications involving membranes or separation processes, where the mass transfer under nonequilibrium conditions plays a predominant role, the determination of the transport diffusivity is of greatest importance. Further, as the D_s and D_t can differ by several orders of magnitude in some porous systems,[44−46] it is of interest to determine these two diffusivities separately. The transport diffusivity is commonly defined in terms of the corrected or jump diffusivity (D_o) by using the Darken equation which implies a thermodynamic correction factor deduced from the adsorption isotherm.[43] Generally, one thus observes that the self-diffusivity, transport diffusivity, and corrected diffusivity for species confined in nanoporous materials depend on the concentration, and they equal only in the limit of dilute concentrations.[42]

The selected material, MIL-47 (V^{4+})[47] which belongs to the MIL (Materials of the Institut Lavoisier) series, is built up from infinite chains of corner sharing $V^{4+}O_4O_2$ octahedra interconnected by 1,4-benzenedicarboxylate groups, creating a 3D framework containing 1D-channels with pores of nanometer dimensions as described in Figure 1. This material has been increasingly investigated for its very promising adsorption/separation properties of various high-impact vapors/gases including alkanes,[28] xylenes,[48] and N_2/CH_4 or N_2/CO_2 mixtures.[49] Further, this solid is also of fundamental interest as it has been shown that (i) the synthesized samples

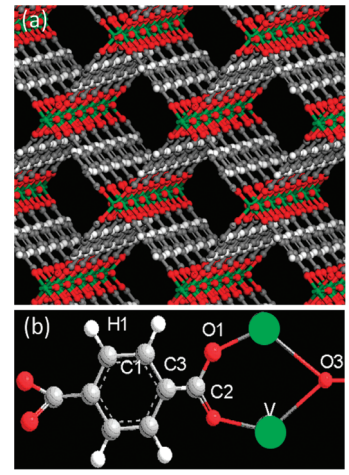

Figure 1. (a) View of the MIL-47(V) structure along the chain (*z* axis), highlighting the 1D pores system with an orthorhombic *Pnma* space group. The oxygen atoms linking the metal to each other are called μ_2-O groups. (b) Labels of the different atoms of the MIL-47(V) structure.

can be well activated; that is, the accessible pores do not contain any organic solvent which would drastically affect the adsorption/diffusion of guest species and (ii) the crystal structure remains unchanged upon inclusion of gas molecules.[24,50,51] Both aspects constitute a great opportunity to validate a joint experimental−theoretical methodology in order to investigate the dynamics of a probe molecule in an "ideal" system which would further be transferred to more complex solids such as the flexible MIL-53 solids.

From an experimental point of view, quasi-elastic neutron scattering (QENS) has already been successfully used to follow the self-diffusivities of H_2 and CH_4 in MOFs,[23,24,50] and will be employed to extract the transport diffusivity (D_t) of CO_2 in MIL-47(V) for a wide range of loading. Molecular dynamics simulations will be then conducted to compute both self-diffusivity (D_s) and corrected (D_o) diffusivity and further elucidate the diffusion mechanisms at the microscopic scale. These calculations are based on interatomic potential parameters[52] for describing the interactions between CO_2 and the MIL-47(V) framework which will be preliminary validated on the thermodynamics of this system *via* a comparison between grand canonical Monte Carlo simulations and manometry measurements. The determination of the thermodynamic correction factors from the adsorption isotherm further will allow a comparison between the experimental and simulated evolutions of D_o and D_t as a function of the pore loading.

RESULTS AND DISCUSSION

The QENS spectra reported in Figure 2 were obtained at different CO_2 concentrations for the same wave-vector transfer. The quality of the spectra is much higher than in the flexible MIL-53(Cr) framework,[53] and the mean error for D_t is down to 20%. It can be noted in

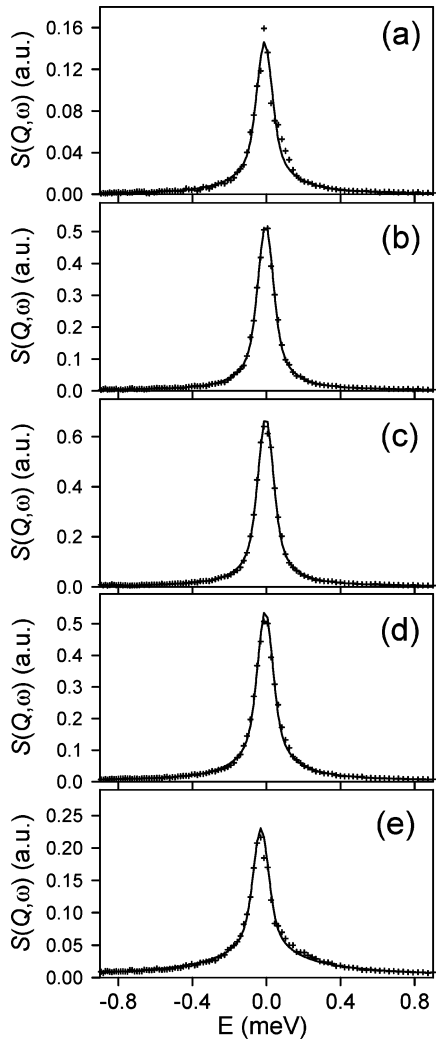

Figure 2. Comparison between experimental (crosses) and fitted (solid lines) QENS spectra obtained for different concentrations of CO_2 in MIL-47(V): (a) 0.84, (b) 2.7, (c) 4, (d) 6, (e) 8.6 molecules per unit cell (T = 230 K, Q = 0.35 Å^{-1}).

Figure 2 that the intensity increases, reaches a maximum for the intermediate loading, and then decreases. To understand this intensity variation, one has to take into account that carbon and oxygen atoms are coherent scatterers, so that the scattering of CO_2 is totally coherent. The observed intensity is proportional to the structure factor, *S(Q)*, which decreases at low *Q* when the loading increases, multiplied by the number of scattering molecules.[42,45] This results in an intensity maximum at intermediate loading. At saturation, the intensity should reach zero. Since there is no contribution from rotation for this coherent scatterer, the spectra could be fitted with a Lorentzian function corresponding to translational motion, convoluted with the instrumental resolution. The profiles could be fitted equally well with 1D or 3D diffusion, so there is no clear indication of anisotropy from the neutron data. The broadenings of the elastic peaks were found to increase with increasing *Q* value (*e.g.*, Figure 3) indicating a long-range diffusion process. Note however, that since the scattering from CO_2 is only coherent, one probes the transport diffusion, D_t.[42] The experimental D_t values are reported in Figure 4. They follow a nonmonotonous evolution with the pore loading, slightly decreasing at low CO_2 concentration prior to significantly increasing from 4.0 to 8.6 CO_2/u.c. These D_t values are comparable to those observed for the isostructural large pore form of MIL-53(Cr)[53] which is consistent with a similar strength of interactions between CO_2 and both MIL frameworks.[31,33,38] Further, the profile and the absolute values for D_t are similar to those previously predicted by Skoulidas *et al.* in the MOF-5 system, while we observe a more pronounced increase at higher loading.[39]

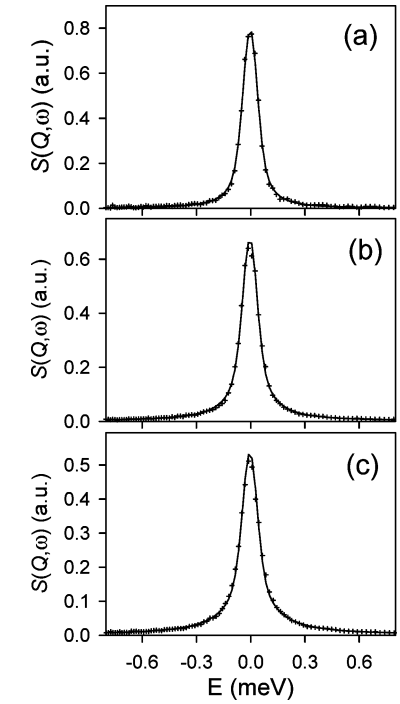

Figure 3. Comparison between experimental (crosses) and fitted (solid lines) QENS spectra obtained at different wavevectors for CO_2 in MIL-47(V), for a concentration of four molecules per u.c.: (a) 0.27, (b) 0.35, (c) 0.42 Å^{-1} (T = 230 K).

The corrected diffusivities (D_o) have been further determined by correcting the transport diffusivities by the

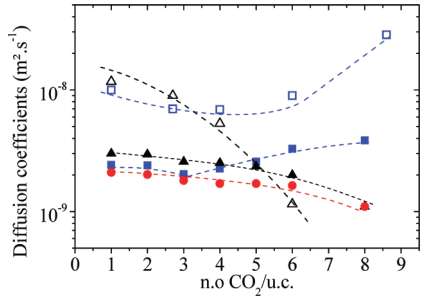

Figure 4. Evolution of the experimental D_o (black △) and D_t (blue □) and of the simulated D_s (red ●), D_o (black ▲) and D_t (blue ■) as a function of the CO_2 concentration in MIL-47(V). The error bars for the simulations are 16%, 7%, and 12% for low, intermediate, and high loading, respectively, while the experimental data are defined within an average error bar of 20%.

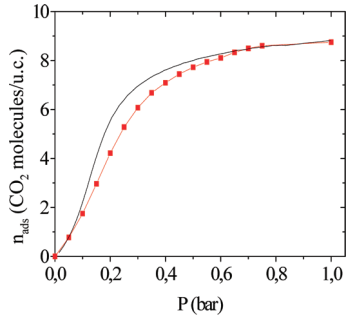

Figure 5. Simulated (red squares) and experimental (black line) CO_2 adsorption isotherms for MIL-47(V) at 230 K.

thermodynamic correction factors (Γ), calculated from the experimental CO_2 adsorption isotherm measured at 230 K (Figure 5) *via* eq 3. The resulting D_o values are reported in Figure 4 from the Γ values determined for the different investigated CO_2 loadings (Figure 6). One observes that D_o decreases when the pore loading increases, as previously observed in various adsorbate/zeolite system including CF_4 in silicalite.[54] Such behavior has been also reported by a joint QENS-molecular simulation study on the CO_2/silicalite system, and it has been ascribed to an increase of the adsorbate−adsorbate interaction when the loading increases.[55] From a general perspective, corrected diffusivities obtained by QENS for several zeolite systems display varying concentration dependences.[42] Here, we show that at low loading (i) the D_o values are unusually higher than the D_t ones, and (ii) the D_t values decrease which has been never observed so far in microporous systems. Both peculiarities are caused by the unusual value of Γ which passes below 1 in this range of loading (Figure 6). Such behavior of Γ which differs from that usually observed in zeolites has already been predicted in MOFs although never clearly explained.[39,56] In our case, this should be related to the inflection of the adsorption isotherm below 0.1 bar (Figure 5), which differs from the convex shape of the I-type isotherm most commonly observed for the zeolites microporous systems. To confirm this assumption, Grand Canonical Monte Carlo (GCMC) simulations were performed to calculate the absolute CO_2 adsorption isotherm for MIL-47(V) at 230 K in the low domain of pressure up to 1 bar. As seen in Figure 5, our GCMC simulations reproduce very well the experimental adsorption isotherm over the whole range of pressure and more particularly the inflection observed at the initial stage of loading. In addition to a validation of the force field used for describing the host/guest interactions, these calculations allowed us to interpret at the microscopic scale the presence of such an inflection at low loading by the occurrence of two different subregimes: (i) an adsorption of CO_2 close to the MIL-47(V) pore wall, mainly in interaction with the carboxylate group at the beginning of the adsorption and further (ii) a preferential sitting of the adsorbate molecules in the center of the pore at higher pressure due to the strong interaction between adsorbate molecules themselves. In addition, our simulations confirm that Γ reaches values slightly below 1 for loadings lower than 5 CO_2/u.c. as illustrated in Figure 6. Further, a direct evaluation of the thermodynamic correction factors can be made from the scattered neutron intensities.[57] However, the Γ values have to be normalized. In our case, the normalization was made with respect to the lowest concentration. The obtained values shown in Figure 6 have a similar trend to the points derived from the experimental or simulated adsorption isotherms, but one cannot check if Γ goes below 1. Note that, when Γ is smaller than 1, the limit of $S(Q)$ at zero wavevector transfer, which is the inverse of Γ,[42] attains values above 1. The largest value of $S(Q)_{Q\to 0}$ is normally 1, it is obtained for a perfect gas. This indicates that the CO_2 molecules, because of attractive intermolecular interactions, in MIL-47(V) behave like an ideal gas.

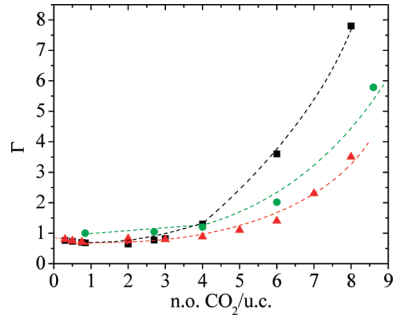

Figure 6. Evolution of the experimental (black ■ and green ● symbols obtained from adsorption isotherms and neutrons experiments, respectively) and simulated (red ▲ symbols) thermodynamic correction factors as a function of the CO_2 loading calculated at 230 K.

The fair agreement obtained between the experimental and simulated thermodynamics properties of the system of interest led us to transfer the force field to the investigation of the dynamics in order to propose some molecular insight on the diffusion of CO_2 in the MIL-47(V) material. Molecular dynamics simulations were thus performed to follow the loading dependence of the self-diffusivity, corrected diffusivity, and transport diffusivity and then to further elucidate the diffusion mechanism of CO_2 at the microscopic scale. The self-diffusivity has first been simulated as a function of the pore loading (Figure 4). D_s slightly decreases as the CO_2 loading increases due mainly to steric hindrance, with the characteristic d(CO_2−CO_2) distance between the adsorbate molecules becoming significantly shorter. As mentionned above, these simulated D_s values can not be compared to the experimental ones as the D_s is not accessible from QENS since CO_2 is a coherent scatterer. However, one can notice that this evolution is in accordance with that already reported for other MOFs and zeolites.[40−42] A further step consisted of calculating the loading dependence of the corrected diffusivity which can thus be compared to the experimental data (Figure 4). Our simulations thus confirm that D_o does not remain constant in the concentration

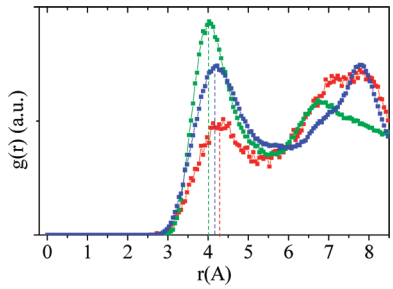

Figure 7. Radial distribution function for the CO_2-CO_2 pair calculated from our MD simulations as a function of the CO_2 loading (red, 2CO_2/u.c.; blue, 4CO_2/u.c.; green, 8CO_2/u.c.).

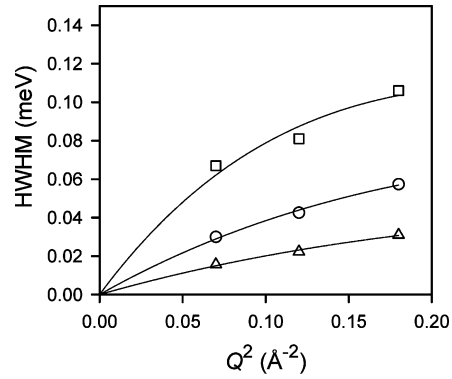

Figure 8. Half-width at half-maxima (HWHM) of the spectra as a function of Q^2 for a concentration of 4 CO_2 per u.c., at different temperatures: (□) 260, (○) 230, (△) 200 K. The symbols are obtained from individual fits of the spectra, the curves with simultaneous fits using a jump diffusion model.

range studied, showing a decreasing profile which deviates with those previously predicted in other MOFs.[39,40,43,57,58] While our simulations fairly reproduce both experimental trend and absolute D_o values at intermediate and high CO_2 loading, they lead to an underestimation of the values at low coverage; however, one should keep in mind that a forcefield validated on the thermodynamics properties of the investigated system (Figure 5) does not always guarantee that the dynamics features would match perfectly the experimental data as we have previously pointed out for other adsorbate/MOFs systems.[24] The decreasing evolution of D_o as a function of the loading is mainly due to an increase of the adsorbate/adsorbate interaction when the CO_2 concentration increases as illustrated by the radial distribution function (CO_2/CO_2) reported in Figure 7, which evidences that the distance between CO_2 molecules decreases when the loading increases. Such increasing attraction between the adsorbate molecules can explain the decreasing profile of D_o. The transport diffusivities in the whole range of CO_2 loading was then computed by multiplying the simulated D_o values by the thermodynamic correction factors (Figure 6) estimated from the simulated adsorption isotherm (Figure 5). The resulting simulated D_t values are reported and compared to the experimental ones in Figure 4. One can observe that the D_t profile is in good accordance with the experimental data (Figure 4), which start with a slight decrease at low CO_2 concentration followed by a significant increase above 3 CO_2/u.c. One can notice that the position of the minimum for D_t is slightly shifted to lower CO_2 concentration in the case of our simulations. Further, the experimental absolute values are underestimated by a factor of 2 and 7 at low and high CO_2 concentrations, respectively. This discrepancy can be explained by the same reasons above invoked for D_o. Finally, one can also observe that at the limit of zero concentration of the adsorbate, the two quantities D_t and D_o become almost equal consistent with a Γ value close to 1 (Figure 6), and further only slightly differ from the D_s value.

Further, for a CO_2 concentration of 4.0 molecules per unit cell, spectra were measured at three different temperatures. The HWHM values (half-width at half-maxima) extracted from the spectra obtained at low Q values are reported in Figure 8. The broadenings increase when the temperature increases, indicating a higher diffusivity. Fickian diffusion yields a straight line when the broadening is plotted as a function of Q^2. The deviation from the straight line observed in Figure 8 reveals that elementary diffusive steps are being probed on a length scale of $2\pi/Q$. The resulting activation energy of 10.3 kJ · mol^{-1} (Figure 9a) is similar to that previously observed (9.7 kJ · mol^{-1}) for the MIL-53(Cr) material loaded with the same CO_2 concentration[53] which is again consistent with very similar adsorption enthalpies measured in both solids.[31,33,38] In parallel, an activation energy of 6.4 kJ · mol^{-1} (Figure 9b) was calculated for the loading of 4 CO_2/u.c., which is significantly higher than those previously determined for CH_4 (3.0 kJ · mol^{-1})[50] and H_2 (0.6 kJ · mol^{-1})[23,24] in the same MIL-47(V)[23,24,49] system consistent with the following sequence of the self-diffusivity, D_s (CO_2) < D_s (CH_4) < D_s (H_2), as well as the strongest energetic interaction for CO_2 compared with the other adsorbate molecules.[51] One should notice that the simulated activation energy is slightly different with those experimentally determined, as the forcefield we used was not preliminary fitted to reproduce the energetics of the system. Further, the activation energy calculated for D_o at the same loading from Figure 9c (6.7 kJ · mol^{-1}) does not significantly differ from the one simulated for the self-diffusivity and remains lower than the experimental one estimated for D_o.

Finally, to clarify the microscopic diffusion mechanism which was not unambiguously elucidated from the QENS measurements, the probability density of CO_2 within the pore of MIL-47(V) were calculated from the analysis of the configurations stored during the MD runs at 230 K. The corresponding density plots through the (*xy*) plane are reported in Figure 10a,b at low (2 CO_2/u.c.) and high (7 CO_2/u.c.) loadings, respectively. A broader probability distribution within the pore is ob-

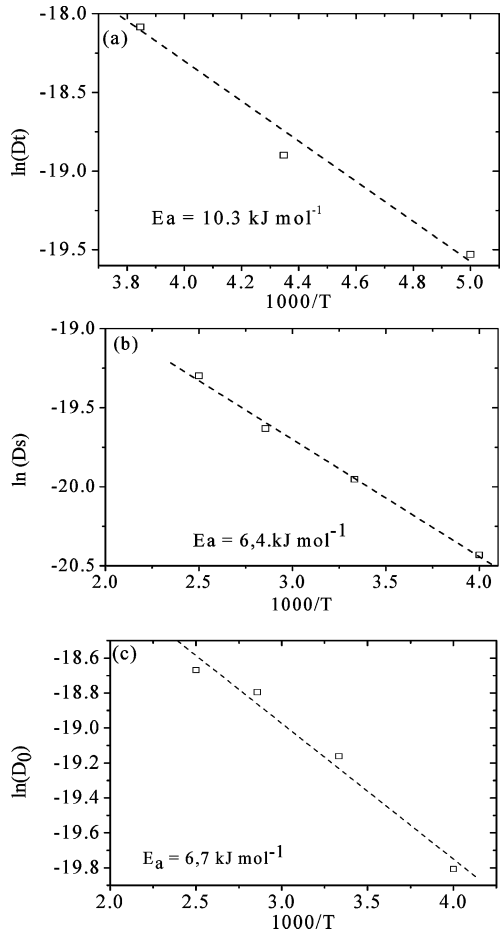

Figure 9. Arrhenius plots of the transport diffusivity (a), self-diffusivity (b), and corrected diffusivities (c) of CO_2 as obtained by QENS (D_t) and MD (D_s and D_o) under the same conditions of loading, *i.e.*, 4 CO_2 molecules/u.c. The activation energies extracted from the plots are provided for comparison.

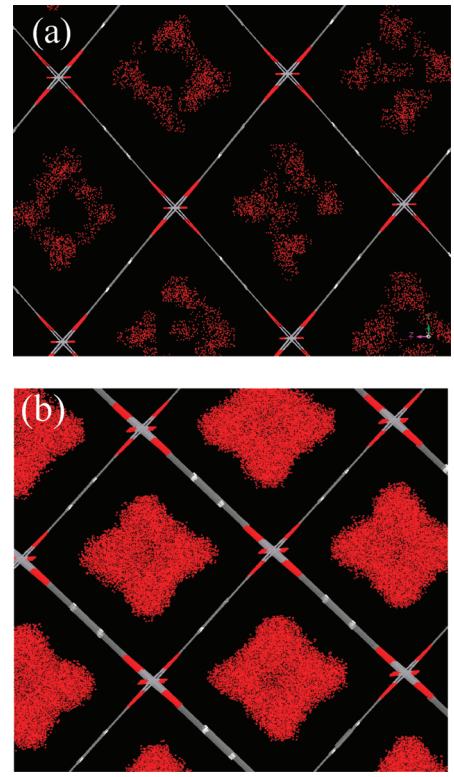

Figure 10. Typical illustration of the 3D microscopic diffusion mechanism of CO_2 in MIL-47(V) at (a) low loading (2 CO_2/u.c.) and (b) high loading (7 CO_2/u.c.) from the 2D probability density plots calculated from our MD simulations.

tained whatever the loading, thus suggesting a purely 3D diffusion mechanism within the tunnel which was also confirmed by the visual inspection of the MD trajectories. Further, our simulations do not show any transition of the CO_2 molecules from one pore to another through the wall mainly due to the orientation of the phenyl rings which lie parallel to the inorganic chain. The displacement of the CO_2 molecules along the *xy* axis are thus only limited within the same pore. This dynamic behavior is thus consistent with that previously pointed for H_2 in MIL-47(V) while it deviates from the 1D type diffusion mechanism observed for CH_4 in the same system.

CONCLUSION

The self- corrected and transport diffusivities of CO_2 have been investigated in the rigid MIL-47(V) MOF using a combination of QENS measurements and MD simulations. The force field used for describing the host/guest interactions was first validated on the thermodynamics of the system. This then led to simulated CO_2 dynamic properties as a function of the pore loading in good agreement with those determined by our QENS measurements. While D_s and D_o exhibit a decreasing profile, D_t presents a non monotonous trend with a slight decrease at low loading followed by a sharp increase at higher loading. This later atypical behavior has been ascribed to the unusual evolution of the thermodynamic correction factor which reaches values below 1 at low loading. Finally, analyses of MD trajectories allow an elucidation of a 3D diffusion mechanism within the pore of the MIL-47(V). This study which comes as an extension of our previous works dedicated to the self-diffusion of various adsorbates in MOF materials,[23,24,41] unambiguously shows that our joint QENS-MD approach is also able to probe the transport diffusivity in MOFs. This strategy can be thus used to explore the diffusion behavior of guest molecules included in a wide variety of MOFs and more particularly the dynamics of industrially important gas mixtures which can play a crucial role on the selectivity of MOFs as new sorbents.

TABLE 1. Atomic Partial Charges (in Electron Units) Carried by the Different Atoms within the MIL-47(V)) Framework, the Labels of the Atoms Being Described in Figure 1

atoms:	H1	C1	C3	C2	01	V	μ_2_o = 03
charges	0.146	−0.071	−0.068	0.604	−0.496	1.207	−0.596

MODELS AND METHODS

Sample Preparation. MIL-47(V) was synthesized and activated according to the published procedures.[47] Hydrogenated MIL-47 was used for the *in situ* XRD analysis and the isotherm measurement, whereas deuterated MIL-47(V) was selected for the neutrons scattering experiments. This latter was prepared from d_4-terephthalic acid (Euristotop, France) and hydrogenated solvent as already reported.[47]

Manometry Measurements. The adsorption of carbon dioxide was carried out at 230 K up to 1 bar for the MIL-47(V) system using a manometric adsorption apparatus.[59] This experimental device measures the isotherms using a point by point introduction of gas to the sample. Prior to each adsorption experiment, the samples were outgassed at 200 °C under a vacuum of 10^{-3} mbar. The carbon dioxide gas was obtained from Air Liquide and was of purity 99.998% (N48). Each experiment was repeated several times and the isotherms were obtained by averaging over all four experiments. This leads to an incertitude of less than 0.1%.

***In Situ* Synchrotron X-ray Powder Diffraction.** The *in situ* synchrotron X-ray powder diffraction (XRPD) experiments[60] were carried out at the Swiss−Norwegian Beamline BM01A in the European Synchrotron Radiation Facility. A 0.7 mm quartz capillary was filled with the sample (MIL-47(V)) and attached to a gas manifold, using MAR345 imaging plate at a sample-to-detector distance of 250 mm, $\lambda = 0.710756$ Å. The data were integrated using Fit2D program (Dr. A. Hammersley, ESRF) and a calibration measurement of a NIST LaB6 standard sample.

X-ray diffraction powder pattern of MIL-47 (V) under CO_2 atmosphere was recorded at 200 K from 0 to 1.53 bar for CO_2. The X-ray diffractograms were indexed (orthorhombic, space group *Pnma* (No. 62)) and refined with a structureless pattern profile using the DICVOL,[61] FULLPROF[62] software and the graphical interface WINPLOTR.[63] The unit cell parameters and unit cell volume of MIL-47 (V) varied less than 1% with the gas pressure as reported in Table 3, indicating that this material does not breathe significantly within the pressure range studied and thus justifying the rigid structural model used for the simulation.

Quasi-elastic Neutron Scattering Measurements. The neutron experiments were performed at the Institut Laue-Langevin, Grenoble, France, using the time-of-flight (TOF) spectrometer IN6. The main characteristics of this instrument are an intermediate elastic resolution (of the order of 80 μeV, full-width at half-maximum, for an incident energy of 3.12 meV), but a very high flux which is obtained by vertical and horizontal focusing. After scattering from the sample, the neutrons pass through a box filled with helium toward a bank of detectors covering a range of scattering angles $10° < 2\theta < 115°$. The corresponding elastic wave-vector transfers, Q, range from 0.21 to 2.1 Å^{-1}. The TOF spectra were grouped into several Q-space regions, avoiding the Bragg peaks of MIL-47(V). The Bragg peaks of the MOF were determined on the spectrometer by comparing the intensities of the elastic peaks at each angular position with those obtained from a standard vanadium plate (vanadium was also used to measure the instrumental resolution). Since the scattering from the hydrogen atoms of the benzenedicarboxylate ligands is incoherent, the framework was deuterated to reduce the signal in-between the Bragg peaks. The MIL-47(V) sample was activated by pumping under slow heating up to 473 K (final pressure below 10^{-3} Pa). The MOF was transferred inside a glovebox into a slab-shaped aluminum container, which could be connected to a gas inlet system allowing *in situ* adsorption. After measuring the scattering of the empty MIL-47(V), five successive concentrations of CO_2 were investigated at 230 K, the third loading was studied at three different temperatures to obtain the activation energy for the transport diffusion. The loadings, corresponding to 0.84, 2.7, 4.0, 6.0, and 8.6 CO_2 molecules per unit cell, were determined by volumetry and then compared to the adsorption isotherms measured independently. The groupings of spectra were treated by standard correction programs, subtracting the signal of the empty MIL-47(V), and the TOF axis was converted to energy, $\hbar\omega$ being the energy transfer.

TABLE 2. Interatomic Potential Parameters for Describing the CO_2/CO_2 and CO_2/MIL-47(V) Interactions

atom type	σ_{ii} (Å)	ε_{ii} (kJ · mol^{-1})
c_co2	2.75700	0.233392
o_co2	3.03299	0.66952
03	3.12000	0.71111
02	2.96000	0.87843
C1 /C2/C3	3.61815	0.61842
H1	2.44833	0.16020

TABLE 3. Evolution of the Unit-Cell Parameters of MIL-47 (V) *vs* Applied Pressure (Experimental). All Diffraction Patterns Were Indexed and Refined in the Orthorhombic *Pnma* Space Group

P (bar)	*a* (Å)	*b* (Å)	*c* (Å)	*V* (Å^3)
pristine solid	6.809(1)	16.108(3)	13.924(3)	1527.4(5)
		Solid upon CO_2 Adsorption		
0.24	6.814(1)	16.398(4)	13.599(3)	1519.4(5)
0.53	6.823(1)	16.409(3)	13.608(3)	1523.5(5)
1.03	6.829(1)	16.401(3)	13.623(3)	1525.7(5)
1.53	6.826(1)	16.397(3)	13.628(2)	1525.3(5)

Partial Charges and Interatomic Potential Parameters. The partial charges carried by all the atoms of the MIL-47(V) were taken from our previous DFT calculations,[50] and they are summarized in Table 1, the position of each atom type in the framework being illustrated in Figure 2.

The Lennard-Jones (LJ) parameters for describing the MIL-47(V) framework was derived from our previous investigation[52] dedicated to the isostructural MIL-53(Cr) form, except that we did not consider any LJ contribution for the Vanadium atom as (i) its polarizability is much lower than those of the surrounding oxygen atoms and (ii) its position is shielded by the octahedral arrangement of the oxygen atoms. Regarding the CO_2 molecule, the three-point charge rigid model reported by Harris and Yung model was used.[64] The corresponding partial charges expressed in electron units are 0.6512 and 0.3256 for the C and O atoms, respectively. The CO_2-framework interactions were then modeled considering both Coulombic and LJ interactions. The resulting LJ parameters, calculated using the classical Lorentz−Berthelot mixing rules, are sumarized in Table 2.

Grand Canonical Monte and Molecular Dynamics Simulations. The absolute adsorption isotherm for the MIL-47(V) system was computed up to 1 bar at 230 K using a Grand Canonical Monte Carlo algorithm, as implemented in the sorption module of the Cerius^2 software suite.[65] A simulation box corresponding to 16 unit cells with typically 2.5×10^6 Monte Carlo steps was considered. The framework was kept rigid during the whole adsorption process, in agreement with *in situ* X-ray powder diffraction as described above. The Ewald summation was used for calculating electrostatic interactions, and the short-range interactions were computed with a cutoff distance of 12 Å.

Molecular dynamics simulations were then performed using the DL_POLY program[66] in the NVT ensemble. The Berendsen thermostat was used, and we checked that the Nose−Hoover thermostat led to the same results. The Coulombic interactions were evaluated using the Ewald summation, while the short-

range contributions were computed with a cutoff distance of 12 Å. For each investigated loading, we considered starting configurations previously obtained by GCMC. The calculations were performed at 230 K for 1, 2, 3, 4, 5, 6, 7, and 8 CO_2 molecules per unit cell to be consistent with the range of loading experimentally explored. The MIL-47(V) was considered again as a rigid framework in accordance with the unchanged position of the whole Bragg peaks observed during the QENS experiments upon CO_2 adsorption. Each run was realized for 10×10^6 steps (*i.e.*, 10 ns) with a time step of 1 fs, following 1 ns of equilibration. The configurations were stored every 1000 time steps.

From these simulations, both the self-diffusivity D_s and corrected diffusivity D_o as a function of the pore loading were extracted, which correspond to individual and collective motions of the guest molecules. Both diffusion coefficients were efficiently calculated for each investigated CO_2 concentration (c) from the MD trajectory using Einstein expressions. The self-diffusivity was then calculated *via*[67]

$$D_s(c) = \lim_{t\to\infty} \frac{1}{6t}\left\langle \frac{1}{N}\sum_{j=1}^{N} ||r_j(t) - r_o(0)||^2 \right\rangle \quad (1)$$

where $\langle ... \rangle$ denotes an ensemble average, $r(t)$ are the vector positions of diffusive molecules, and N corresponds to the number of CO_2 molecules in the simulation volume.

The corrected diffusivity as previously reported[39] was calculated by means of an Einstein expression similar to eq 1 that measures the mean square displacement (MSD) of the center of mass of the diffusive molecules:

$$D_o(c) = \frac{1}{6N}\lim_{t\to\infty} \frac{1}{t}\left\langle \sum_{j=1}^{N} ||r_j(t) - r_o(0)||^2 \right\rangle \quad (2)$$

Further, to improve the statistics of the calculation, multiple time origins as described elsewhere[67] were used with an average value over five independent trajectories. For the loading of 4 CO_2/u.c., the calculations were performed at four different temperatures in the range 200−300 K to extract the activation energies from the linear least-squares fit to the Arrhenius plots of $\ln(D_i) = f(1000/T)$ where i = s or o. Finally, the transport diffusivities were calculated from

$$D_t(c) = D_o(c)\left(\frac{\mathrm{d}\ln p}{\mathrm{d}\ln c}\right) \quad (3)$$

where the partial derivative involving the CO_2 concentration (c) and the pressure (p) is defined as the thermodynamic correction factor namely Γ, which was determined from the simulated adsorption isotherm.

Acknowledgment. This work was supported by French programs ANR CO_2 "NoMAC" (ANR-06-CO2-008) and ANR Blanc "SAFHS" (ANR-07-BLAN-0284-03) and by STREP FP6 EU project "DeSANNS". We thank the Institut Laue-Langevin, Grenoble, France, for neutron beam time and Dr M.M. Koza for his help during the experiment, we also thank the Swiss−Norwegian Beamline and the European Synchrotron Radiation Facility (Grenoble, France) for the X-ray beam time and Dr Y. Filinchuk for his help.

REFERENCES AND NOTES

1. Morris, R. E.; Wheatley, P. S. Gas Storage in Nanoporous Materials. *Angew. Chem., Int. Ed.* **2008**, *47*, 4966–4981.
2. Kikkinides, E. S.; Yang, R. T.; Cho, S. H. Concentration and Recovery of Carbon Dioxide from Flue Gas by Pressure Swing Adsorption. *Ind. Eng. Chem. Res.* **1993**, *32*, 2714–2720.
3. Férey, G. Hybrid Porous Solids: Past, Present, Future. *Chem. Soc. Rev.* **2008**, *37*, 191–214.
4. Lopes, F. V. S.; Grande, C. A.; Ribeiro, A. M.; Loureiro, J. M.; Evaggelos, O.; Nikolakis, V.; Rodrigues, A. E. Adsorption of H_2, CO_2, CH_4, CO, N_2, and H_2O in Activated Carbon and Zeolite for Hydrogen Production. *Sep. Sci. Technol.* **2009**, *44*, 1045.
5. Arstad, B.; Fjellvag, H.; Kongshaug, K. O.; Swang, O.; Blom, R. Amine-Functionalized Metal−Organic Frameworks (MOFs) as Adsorbents for Carbon Dioxide. *Adsorption* **2008**, *14*, 755–762.
6. Li, K.; Olson, D. H.; Lee, J. Y.; Bi, W.; Wu, K.; Yuen, T.; Xu, Q.; Li, J. Multifunctional Microporous MOFs Exhibiting Gas/Hydrocarbon Adsorption Selectivity, Separation Capability, and Three-Dimensional Magnetic Ordering. *Adv. Funct. Mater.* **2008**, *18*, 2205–2214.
7. Czaja, A. U.; Turkhan, N.; Müller, U. Industrial Applications of Metal−Organic Frameworks. *Chem. Soc. Rev.* **2009**, *38*, 1284–1293.
8. Murray, L. J.; Dinca, M.; Long, J. R. Hydrogen Storage in Metal−Organic Frameworks. *Chem. Soc. Rev.* **2009**, *38*, 1294–1314.
9. Latroche, M.; Surblé, S.; Serre, C.; Mellot-Draznieks, C.; Llewellyn, P.; Chang, J. S.; Jung, S.-H.; Férey, G. Hydrogen Storage in the Giant-Pore Metal−Organic Frameworks MIL-100 and MIL-101. *Angew. Chem., Int. Ed.* **2006**, *45*, 8227–8231.
10. Han, S. S.; Mendoza-Cortès, J. L.; Goddard, W. A. Recent Advances on Simulation and Theory of Hydrogen Storage in Metal−Organic Frameworks and Covalent Organic Frameworks. *Chem. Soc. Rev.* **2009**, *38*, 1460–1476.
11. Férey, G.; Latroche, M.; Serre, C.; Millange, F.; Loiseau, T.; Percheron-Grégan, A. Hydrogen Adsorption in the Nanoporous Metal−Benzenedicarboxylate M(OH)(O_2C-C_6H_4-CO_2) (M = Al^{3+}, Cr^{3+}) MIL-53. *Chem. Commun.* **2003**, 2976–2977.
12. Rosi, N. L.; Eckert, J.; Eddaoudi, M.; Vodak, D. T.; Kim, J.; O'Keefe, M.; Yaghi, O. M. Hydrogen Storage in Microporous Metal−Organic Frameworks. *Science* **2003**, *300*, 1127–1129.
13. Furukawa, H.; Miller, M. A.; Yaghi, O. M. Independent Verification of the Saturation Hydrogen Uptake in MOF-177 and Establishment of a Benchmark for Hydrogen Adsorption in Metal−Organic Frameworks. *J. Mater. Chem.* **2007**, *17*, 3197–3204.
14. Surblé, S.; Millange, F.; Serre, C.; Düren, T.; Latroche, M.; Bourrelly, S.; Llewellyn, P. L.; Férey, G. Synthesis of MIL-102, a Chromium Carboxylate Metal−Organic Framework, with Gas Sorption Analysis. *J. Am. Chem. Soc.* **2006**, *128*, 14889.
15. Sudik, A. C.; Millward, A. R.; Ockwig, N. W.; Côte, A. P.; Kim, J.; Yaghi, O. M. Design, Synthesis, Structure, and Gas (N_2, Ar, CO_2, CH_4, and H_2) Sorption Properties of Porous Metal−Organic Tetrahedral and Heterocuboidal Polyhedra. *J. Am. Chem. Soc.* **2005**, *127*, 7110–7118.
16. Millward, A. R.; Yaghi, O. M. Metal−Organic Frameworks with Exceptionally High Capacity for Storage of Carbon Dioxide at Room Temperature. *J. Am. Chem. Soc.* **2005**, *127*, 17998–17999.
17. Llewellyn, P. L.; Bourrelly, S.; Serre, C.; Vimont, A.; Daturi, M.; Hamon, L.; de Weireld, G.; Chang, J. S.; Hong, D.-Y.; Hwang, Y. K.; *et al.* High Uptakes of CO_2 and CH_4 in Mesoporous Metal−Organic Frameworks MIL-100 and MIL-101. *Langmuir* **2008**, *24*, 7245–7250.
18. Férey, G.; Serre, C. Large Breathing Effects in Three-Dimensional Porous Materials. *Chem. Soc. Rev.* **2009**, *38*, 1380–1399.
19. Maji, T. K.; Kitagawa, S. Chemistry of Porous Coordination Polymers. *Pure Appl. Chem.* **2007**, *79*, 2155–2177.
20. Serre, C.; Bourrelly, S.; Vimont, A.; Ramsahye, N. A.; Maurin, G.; Llewellyn, P. L.; Daturi, M.; Filinchuk, Y.; Leynaud, O.; Barnes, P.; Férey, G. An Explanation for the Very Large Breathing Effect of a Metal−Organic Framework during CO_2 Adsorption. *Adv. Mater.* **2007**, *19*, 2246–2251.
21. Zhou, W.; Yildirin, T. Lattice Dynamics of Metal−Organic Frameworks: Neutron Inelastic Scattering and First-Principles Calculations. *Phys. Rev. B* **2006**, *74*, 180301.
22. Panella, B.; Hönes, K.; Müller, U.; Trukhan, N.; Schubert, M.; Pütter, H.; Hirscher, M. Desorption Studies of Hydrogen in Metal−Organic Frameworks. *Angew. Chem., Int. Ed.* **2008**, *47*, 2138–2142.

23. Salles, F.; Jobic, H.; Maurin, G.; Koza, M. M.; Llewellyn, P. L.; Devic, T.; Serre, C.; Férey, G. Experimental Evidence Supported by Simulations of Hydrogen Supermobility in Metal−Organic Framework Materials. *Phys. Rev. Lett.* **2008**, 245901.
24. Salles, F.; Kolokolov, D. I.; Jobic, H.; Maurin, G.; Llewellyn, P. L.; Devic, T.; Serre, C.; Férey, G. Adsorption and Diffusion of H_2 in MIL-47(V) and MIL-53(Cr): Comparison between Experimental and Simulation Results. *J. Phys. Chem. C* **2009**, *113*, 7802–7812.
25. Rowsell, J. L. C.; Yaghi, O. M. Effects of Functionalization, Catenation, and Variation of the Metal Oxide and Organic Linking Units on the Low-Pressure Hydrogen Adsorption Properties of Metal−Organic Frameworks. *J. Am. Chem. Soc.* **2006**, *128*, 1304–1315.
26. Bae, Y. B.; Mulfort, K. L.; Frost, H.; Ryan, P.; Punnathanam, S.; Broadbelt, L. J.; Hupp, J. T.; Snurr, R. Q. Separation of CO_2 from CH_4 Using Mixed-Ligand Metal−Organic Frameworks. *Langmuir* **2008**, *24*, 8592–8598.
27. Chowdhury, P.; Bikkina, C.; Gumma, S. Gas Adsorption Properties of the Chromium-Based Metal−Organic Framework MIL-101. *J. Phys. Chem. C* **2009**, *113*, 6616–6621.
28. Finsy, V.; Calero, S.; Garcia-Perez, E.; Merkling, P. J.; Vedts, G.; De Vos, D. E.; Baron, G. V.; Denayer, J. F. M. Low-Coverage Adsorption Properties of the Metal−Organic Framework MIL-47 Studied by Pulse Chromatography and Monte Carlo Simulations. *Phys. Chem. Chem. Phys.* **2009**, *11*, 3515–3521.
29. Dietzel, P. D. C.; Johnsen, R. E.; Fjellvag, H.; Bordiga, S.; Groppo, E.; Chavan, S.; Blom, R. Adsoprtion Properties and Structure of CO_2 Adsorbed on Open Coordination Sites of Metal−Organic Framework Ni_2(dhtp) from Gas Adsorption, IR Spectroscopy and X-ray Diffraction. *Chem. Commun.* **2008**, 5125–5127.
30. Barcia, P. S.; Bastin, L.; Hurtado, E. J.; Silva, J. A. C.; Rodrigues, A. E.; Chen, B. L. Single and Multicomponent Sorption of CO_2, CH_4, and N_2 in a Microporous Metal−Organic Framework. *Sep. Sci. Technol.* **2008**, *43*, 3494–3521.
31. Bourrelly, S.; Llewellyn, P. L.; Serre, C.; Millange, F.; Loiseau, T.; Férey, G. Different Adsorption Behaviors of Methane and Carbon Dioxide in the Isotypic Nanopores Metal Terephthalates MIL-53 and MIL-47. *J. Am. Chem. Soc.* **2005**, *127*, 13519–13521.
32. Coudert, F. X.; Mellot-Draznieks, C.; Fuchs, A. H.; Boutin, A. Prediction of Breathing and Gate-Opening Transitions Upon Binary Mixture Adsorption in Metal-Organic Frameworks. *J. Am. Chem. Soc.* **2009**, *131*, 11329–11331.
33. Ramsahye, N. A.; Maurin, G.; Bourrelly, S.; Llewellyn, P. L.; Loiseau, T.; Férey, G. On the Breathing Effect of a Metal−Organic Framework upon CO_2 Adsorption: Monte Carlo Simulations Compared to Microcalorimetry Experiments. *Chem. Commun.* **2007**, *31*, 3261–3263.
34. Ramsahye, N.; Maurin, G.; Bourrelly, S.; Llewellyn, P. L.; Serre, C.; Loiseau, T.; Devic, T.; Férey, G. Probing the Adsorption Sites for CO_2 in Metal−Organic Frameworks Materials MIL53(Al, Cr) and MIL-47(V) by Density Functional Theory. *J. Phys. Chem. C* **2008**, *112*, 514–520.
35. Walton, K. S.; Millward, A. R.; Dubbeldam, D.; Frost, H.; Low, J. J.; Yaghi, O. M.; Snurr, R. Q. Understanding Inflections and Steps in Carbon Dioxide Adsorption Isotherms in Metal−Organic Frameworks. *J. Am. Chem. Soc.* **2008**, *130*, 406–407.
36. Yang, Q.; Zhong, C. L. Molecular Simulation of Carbon Dioxide/Methane/Hydrogen Mixture Adsorption in Metal−Organic Frameworks. *J. Phys. B* **2006**, *36*, 17776–17783.
37. Llewellyn, P. L.; Maurin, G.; Devic, T.; Loera-Serna, S.; Rosenbach, N.; Serre, C.; Bourrelly, S.; Horcajada, P.; Filinchuk, Y.; Férey, G. Prediction of the Conditions for Breathing of Metal−Organic Framework Materials Using a Combination of X-ray Powder Diffraction, Microcalorimetry, and Molecular Simulation. *J. Am. Chem. Soc.* **2008**, *130*, 12808–12814.
38. Ramsahye, N. A.; Maurin, G.; Bourrelly, S.; Llewellyn, P. L.; Loiseau, T.; Férey, G. Charge Distribution in Metal−Organic Framework Materials: Transferability to a Preliminary Molecular Simulation Study of the CO_2 Adsorption in the MIL-53(Al) System. *Phys. Chem. Chem. Phys.* **2007**, *9*, 1059–1063.
39. Skoulidas, A. I.; Sholl, D. S. Self-Diffusion and Transport Diffusion of Light Gases in Metal−Organic Framework Materials Assessed Using Molecular Dynamics Simulations. *J. Phys Chem. B* **2005**, *109*, 15760–15768.
40. Babarao, R.; Jiang, J. Diffusion and Separation of CO_2 and CH_4 in Silicalite, C-168 Schwarzite, and IRMOF-1: A Comparative Study from Molecular Dynamics Simulations. *Langmuir* **2008**, *24*, 5474–5484.
41. Yang, Q.; Zhong, C.; Chen, J. F. Computational Study of CO_2 Storage in Metal−Organic Frameworks. *J. Phys. Chem. C* **2008**, *112*, 1562–1569.
42. Jobic, H.; Theodorou, D. N. Quasi-elastic Neutron Scattering and Molecular Dynamics Simulation as Complementary Techniques for Studying Diffusion in Zeolites. *Microporous Mesoporous Mater.* **2007**, *102*, 21–50.
43. Papadopoulos, G. K.; Jobic, H.; Theodorou, D. N. Transport Diffusivity of N_2 and CO_2 in Silicalite: Coherent Quasi-elastic Neutron Scattering Measurements and Molecular Dynamics Simulations. *J. Phys. Chem. B* **2004**, *108*, 12748–12756.
44. Skoulidas, A. I.; Ackerman, D. M.; Johnson, J. K.; Sholl, D. S. Rapid Transport of Gases in Carbon Nanotubes. *Phys. Rev. Lett.* **2002**, *89*, 185901.
45. Jobic, H.; Kärger, J.; Bée, M. Simultaneous Measurement of Self- and Transport Diffusivities in Zeolites. *Phys. Rev. Lett.* **1999**, *82*, 4260.
46. Skoulidas, A. I. Molecular Dynamics Simulations of Gas Diffusion in Metal−Organic Frameworks: Argon in CuBTC. *J. Am. Chem. Soc.* **2004**, *126*, 1356–1357.
47. Barthelet, K.; Marrot, J.; Riou, D.; Férey, G. A Breathing Hybrid Organic−Inorganic Solid with Very Large Pores and High Magnetic Characteristics. *Angew. Chem., Int. Ed.* **2002**, *41*, 281.
48. Alaerts, L.; Kirschhock, C. E. A.; Maes, M.; van der Veen, M. A.; Finsy, V.; Depla, A.; Martens, J. A.; Baron, G. V.; Jacobs, P. A.; Denayer, J. E. M.; De Vos, D. E. Selective Adsorption and Separation of Xylene Isomers and Ethylbenzene with the Microporous Vanadium (IV) Terephthalate MIL-47. *Angew. Chem., Int. Ed.* **2007**, *46*, 4293.
49. Liu, B.; Smit, B. Comaprative Molecular Simulation Study of CO_2/N_2 and CH_4/N_2 Separation in Zeolites and Metal−Organic Frameworks. *Langmuir* **2009**, *25*, 5918–5926.
50. Rosenbach, N.; Jobic, H.; Ghoufi, A.; Salles, F.; Maurin, G.; Bourrelly, S.; Llewellyn, P. L.; Devic, T.; Serre, C.; Férey, G. Quasi-elastic Neutron Scattering and Molecular Dynamics Study of Methane Diffusion in Metal−Organic Frameworks MIL-47(V) and MIL-53(Cr). *Angew. Chem., Int. Ed.* **2008**, *47*, 6611–6615.
51. Ramsahye, N. A.; Maurin, G.; Bourrelly, S.; Llewellyn, P. L.; Devic, T.; Serre, C.; Loiseau, T.; Férey, G. Adsorption of CO_2 in Metal−Organic Frameworks of Different Metal Centres: Grand Canonical Monte Carlo Simulations Compared to Experiments. *Adsorption* **2007**, *13*, 461–467.
52. Salles, F.; Ghoufi, A.; Maurin, G.; Bell, R. G.; Mellot-Draznieks, C.; Férey, G. Molecular Dynamics Simulations of Breathing MOFs: Structural Transformations of MIL-53(Cr) upon Thermal Activation and CO_2 Adsorption. *Angew. Chem., Int. Ed.* **2008**, *47*, 8487–8491.
53. Salles, F.; Jobic, H.; Ghoufi, A.; Llewellyn, P. L.; Serre, C.; Bourrelly, S.; Férey, G.; Maurin, G. Transport Diffusivity of CO_2 in the Highly Flexible Metal−Organic Framework MIL-53(Cr). *Angew. Chem., Int. Ed.* **2009**, *48*, 8335–8339.
54. Jobic, H.; Skoulidas, A. I.; Sholl, D. S. Determination of Concentration Dependent Transport Diffusivity of CF_4 in Silicalite by Neutron Scattering Experiments and Molecular Dynamics. *J. Phys. Chem.B* **2004**, *108*, 10613–10616.

55. Jobic, H.; Makrodimitris, K.; Papadopoulos, G. K.; Schober, H.; Theodorou, D. N. Diffusivities of CO_2 and N_2 in Silicalite, Comparison between Quasi-elastic Neutron Scattering and Molecular Simulations. *Stud. Surf. Sci. Catal.* **2004**, *154*, 2056–2061.
56. Chmelik, C.; Kärger, J.; Wiebcke, M.; Caro, J.; van Baten, J. M.; Krishna, R. Adsorption and Diffusion of Alkanes in CuBTC Crystals Investigated Using Infrared Microscopy and Molecular Simulations. *Microporous Mesoporous Mater.* **2009**, *117*, 22–32.
57. Jobic, H.; Laloué, N.; Laroche, C.; van Baten, J. M.; Krishna, R. Influence of Isotherm Inflection on the Loading Dependence of the Diffusivities of *n*-Hexane and *n*-Heptane in MFI Zeolite. Quasi-elastic Neutron Scattering Experiments Supplemented by Molecular Simulations. *J. Phys. Chem. B* **2006**, *110*, 2195–2201.
58. Jobic, H.; Kärger, J.; Bée, M. Simultaneous Measurement of Self- and Transport Diffusivities in Zeolites. *Phys. Rev. Lett.* **1999**, *82*, 4260–4263.
59. Llewellyn, P. L.; Maurin, G. Gas Adsorption Microcalorimetry and Modelling to Characterise Zeolites and Related Materials. *C.R. Chim.* **2005**, *8*, 283–302.
60. Llewellyn, P. L.; Horcajada, P.; Maurin, G.; Devic, T.; Rosenbach, N.; Bourrelly, S.; Serre, C.; Vincent, D.; Loerna-Serna, S.; Filinchuk, Y.; Férey, G. Complex Adsorption of Short Linear Alkanes in the Flexible Metal−Organic Framework MIL-53(Fe). *J. Am. Chem. Soc.* **2009**, *131*, 13002–13008.
61. Altomare, A.; Caliandro, R.; Camalli, M.; Cuocci, C.; Giacovazzo, C.; Moliterni, A. G. G.; Rizzi, R. Automatic Structure Determination from Powder Data with EXPO2004. *J. Appl. Crystallogr.* **2004**, *37*, 1025.
62. Rodriguez Carvajal, J. Fullprof Suite, LLB Saclay & LCSIM Rennes, France, 2005. http://www.ill.eu/sites/fullprof/php/programs.html.
63. Roisnel, T.; Rodriguez-Carjaval, J. WinPLOTR: A Windows Tool for Powder Diffraction Pattern Analysis. *Mater. Sci. Forum* **2001**, *118*, 378.
64. Harris, J. G.; Yung, K. H. Carbon Dioxide Liquid−Vapor Coexistence Curve and Critical Properties as Predicted by a Simple Molecular Model. *J. Phys. Chem.* **1995**, *99*, 12021–12024.
65. Cerius^2, version 4.0; Accelrys Inc.: San Diego, CA, 1999.
66. Smith, W.; Forester, T. R. DL_POLY_2.0: A General-Purpose Parallel Molecular Dynamics Simulation Package. *J. Mol. Graph.* **1996**, *14*, 136.
67. Frenkel, D., Smit, B., *Understanding Molecular Simulation*; Academic Press:San Diego, CA, 1996.